Research Square

Preprints are preliminary reports that have not undergone peer review.
They should not be considered conclusive, used to inform clinical practice,
or referenced by the media as validated information.

Low-cost smartphone-assisted dual-readout glucose sensing on rosin-patterned paper using Fe(II)/silane-derived carbon dots

Lian-Lian Duan
Hebei University
Chu-Qi Zhang
Hebei University
Yi-Fan Da
Hebei University
Meng-Xi Hao
Hebei University
Zhen-Guang Wang
Hebei Normal University
Li-Qing Yu
Hebei University
Yun-Kai Lv
lvyunkai@126.com

Hebei University

Research Article

Keywords: Fluorescence, Colorimetric, Glucose determination, Fenton reaction, RGB analysis

Posted Date: November 12th, 2026

DOI: https://doi.org/10.21203/rs.3.rs-11337777/v1

License: This work is licensed under a Creative Commons Attribution 4.0 International License.
Read Full License

Additional Declarations: No competing interests reported.

Low-cost smartphone-assisted dual-readout glucose sensing on rosin-patterned paper using Fe(II)/silane-derived carbon dots

Lian-Lian Duan[a], Chu-Qi Zhang[a], Yi-Fan Da[a], Meng-Xi Hao[a], **Zhen-Guang Wang[b]***, Li-Qing Yu[a], **Yun-Kai Lv[a]***

[a] Key Laboratory of Medicinal Chemistry and Molecular Diagnosis of Ministry of Education, Key Laboratory of Analytical Science and Technology of Hebei Province, College of Chemistry and Materials Science, Hebei University, Baoding, 071002, China

[b] College of Chemistry and Materials Science, Hebei Normal University, Shijiazhuang, 050024, China

* Corresponding author: E-mail: lvyunkai@hbu.edu.cn (Y. K. Lv) and zgwang@hbu.edu.cn (Z. G. Wang).

ABSTRACT

A smartphone-assisted dual-readout paper-based sensor was developed by integrating an Fe(II)/silane-derived carbon dot system (Fe(II)/CDs), a rosin-defined hydrophobic detection zone, and Python-based RGB analysis. Glucose was oxidized by glucose oxidase to generate H_2O_2, which subsequently initiated the Fenton reaction. In the fluorescence readout mode, the resulting Fe^{3+} interacted with amino and/or oxygen-containing groups on the carbon-dot surface, leading to fluorescence quenching. In the colorimetric readout mode, Fe^{3+} and hydroxyl radicals promoted the oxidation of TMB to blue oxTMB, while complexation of Fe^{3+} with surface functional groups of the CDs might further facilitate H_2O_2 activation and enhance the colorimetric response. Images from the two readout modes were separately acquired using a smartphone and quantified using the normalized blue-channel fraction, B/(R + G + B). Under optimized conditions, both modes exhibited linear responses to glucose over 0.01–1.00 mM. The fluorescence and colorimetric modes achieved limits of detection of 2.9 and 2.5 μM and limits of quantification of 9.7 and 8.3 μM, respectively. Spike-recovery analysis in tenfold-diluted human serum produced recoveries of 90.00-91.67% for the fluorescence mode and 95.00-105.00% for the colorimetric mode, with relative standard deviations below 3.40% and 4.29%, respectively. Furthermore, the results were auxiliary verified using fluorescence and ultraviolet instruments. The proposed method provides dual quantitative readouts for glucose determination in diluted human serum samples.

KEY WORDS: Fluorescence; Colorimetric; Glucose determination; Fenton reaction; RGB analysis

Introduction

Diabetes is a chronic metabolic disease affecting hundreds of millions of people worldwide. According to data from the International Diabetes Federation (IDF), the global burden of diabetes continues to rise, with the number of affected people projected to reach 643 million by 2030 and increase to 783 million by 2045 [1]. Hyperglycemia is not only a hallmark pathological feature of diabetes but also a key diagnostic indicator. Early monitoring of blood glucose levels facilitates the timely diagnosis and management of diabetes, thereby helping to reduce the risk of associated complications, including cardiovascular disease, neurological damage, and renal failure[2]. Consequently, analytical platforms capable of providing low-cost and decentralized glucose testing have attracted increasing attention for clinical diagnostics, particularly in resource-limited settings[3,4]. However, although fluorescence and colorimetric methods offer the respective advantages of high sensitivity and intuitive visual readout, measurements typically require specialized instrumentation and may therefore be impractical in resource-limited settings. Meanwhile, single-channel measurements remain susceptible to variations in illumination and operation as well as sample matrix effects, making reliable quantitative analysis outside centralized laboratories challenging[5,6]. Smartphone-based digital image analysis offers a rapid, low-cost, and readily implementable approach for quantitative optical sensing[7]. On this basis, the development of sensor interfaces capable of generating multiple optical responses through simple fabrication strategies may further enhance analytical reliability and accessibility.

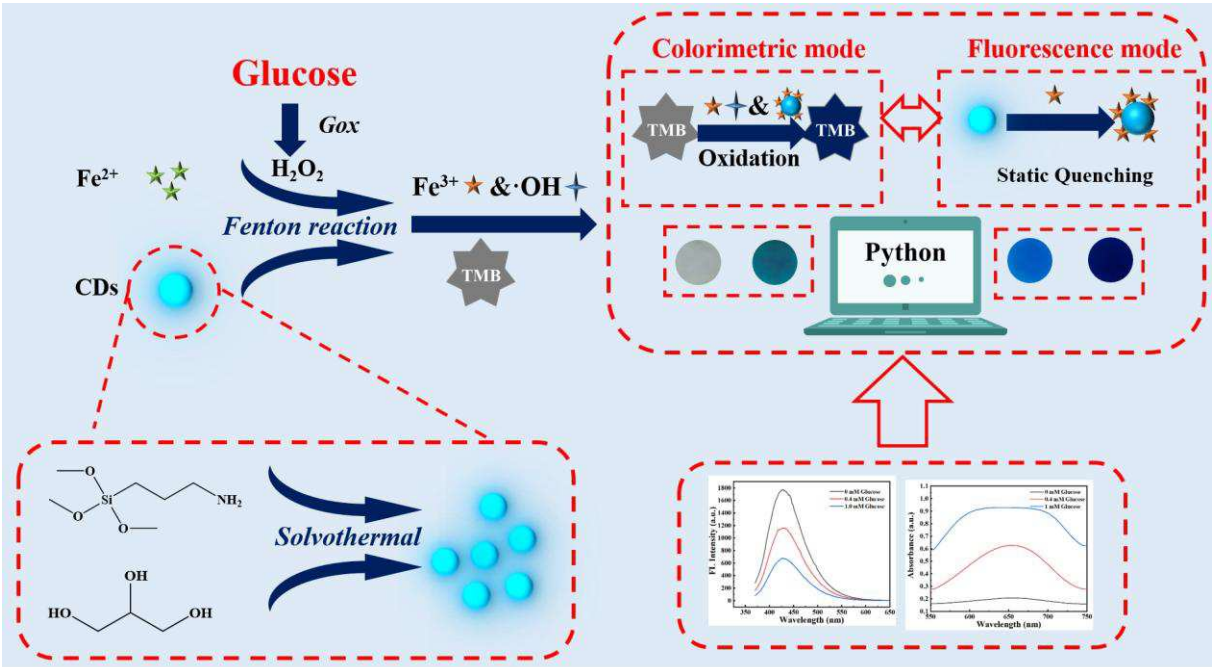
Fluorescence–colorimetric dual-mode optical sensing provides two complementary signal channels within a single analytical system, combining the high sensitivity of fluorescence detection with the intuitive and convenient readout of colorimetric detection. Comparing the results obtained from both modes for the same sample can help reduce erroneous conclusions arising from the susceptibility of a single signal to background interference, fluctuations in illumination, or matrix effects, thereby improving the reliability of analytical results [8]. Various functional nanomaterials, including metal–organic frameworks, metal oxides, noble metal nanoparticles, and carbon-based nanomaterials, have been explored for constructing such dual-readout systems [9–12]. Carbon dots (CDs), a class of carbon-based nanomaterials, offer a versatile platform for constructing functional optical interfaces owing to their tunable photoluminescence, abundant surface functional groups, excellent photostability,

and facile synthesis [13–15]. In particular, silane-derived CDs are rich in amino and oxygen-containing groups, which can serve as both fluorescence-active sites and coordination sites for metal ions [16–18]. Such metal–CD interactions provide opportunities to integrate molecular recognition, catalytic modulation, and optical signal transduction at a single nanoscale interface. However, reported dual-readout platforms require the prior synthesis of metal oxide–CD hybrids or multimetal-doped CDs. Their implementation for portable detection may also involve specialized 3D-printed smartphone accessories or the co-immobilization of natural enzymes, nanozymes, and chromogenic substrates on customized supports [11,12,19,20]. These additional material preparation and device assembly steps may increase fabrication complexity and pose challenges to the scalable production of low-cost, disposable analytical devices.

Iron-based catalytic systems have been extensively investigated for optical sensing owing to their distinctive redox properties and Fenton catalytic activity. The interconversion between Fe(II) and Fe(III) can regulate the generation of hydroxyl radicals (·OH) [21], providing an effective route for signal amplification in colorimetric detection. Meanwhile, Fe(III) can interact with functional groups on CD surfaces and potentially modulate their fluorescence through coordination-induced electronic effects [18]. Accordingly, iron–CD coordination interfaces offer the prospect of an integrated platform that combines fluorescence modulation with catalytic color development. Recent studies have demonstrated that iron-containing CDs can function as both fluorescent probes and peroxidase-like catalysts. For example, Fe–CD systems can generate fluorescence recovery and colorimetric fading responses through changes in the oxidation state of iron [22], whereas Fe/Co bimetal-doped CDs enable fluorescence–colorimetric dual-mode sensing through the catalytic formation of oxidized TMB (oxTMB) and its inner filter effect [23]. These findings establish the feasibility of dual-mode detection using iron-containing CDs. Further development therefore calls for simplifying material preparation, reducing mechanistic coupling between the two signal channels, and translating the sensing chemistry into low-cost, disposable platforms for portable quantitative analysis.

Inspired by these considerations, this study synthesized organosilane-derived carbon dots (CDs) through a one-step thermal treatment and combined them with Fe(II) by simple mixing to construct a Fe(II)/CDs fluorescence–colorimetric dual-readout sensing platform. Glucose oxidation catalyzed by glucose oxidase generates H_2O_2, which subsequently drives the conversion of Fe(II) to Fe(III) and the generation of·OH, coupling

enzymatic recognition with the Fenton reaction to enable cascade transduction from the analyte to optical signals and catalytic signal amplification. In the TMB-free fluorescence readout mode (FRM), the generated Fe(III) interacts with amino and/or oxygen-containing groups on the CD surfaces, decreasing their fluorescence intensity through static quenching. In the colorimetric readout mode (CRM), ·OH and Fe(III) generated during the Fenton reaction promote TMB oxidation to blue oxTMB, while interactions between Fe(III) and CD surface functional groups may further modulate H_2O_2 activation, thereby enhancing the colorimetric response. Therefore, this design reduces direct mechanistic coupling and signal crosstalk between the two channels, improving the complementarity and reliability of the dual-readout results. Furthermore, the readily prepared Fe(II)/CDs sensing system was integrated with manually fabricated, rosin-patterned hydrophobic paper substrates without requiring specialized fabrication equipment. Smartphone-acquired fluorescence and colorimetric images were analyzed in Python using the same normalized blue-channel parameter, B/(R+G+B). Together, these strategies establish a dual-mode analytical platform for disposable, low-cost, and portable quantitative detection (Scheme 1).



Scheme 1 Schematic illustration of the colorimetric/fluorescence detection mechanism for glucose based on Fe(II)/CDs

Experimental

Reagents and chemicals

(3-Aminopropyl)trimethoxysilane (APTMS) was purchased from Shanghai Bangcheng Chemical Co., Ltd. Glycerol was obtained from Tianjin Fuyu Fine Chemical Co., Ltd. Ferrous sulfate was purchased from Tianjin Hengxing Chemical Reagent Manufacturing Co., Ltd. Glucose (Glu), ascorbic acid (AA) and sodium chloride (NaCl) were purchased from Tianjin Kemiou Chemical Reagent Co., Ltd. 3,3',5,5'-Tetramethylbenzidine (TMB), glucose oxidase (GOx), rosin, uric acid (UA) and ferric chloride were purchased from Shanghai Macklin Biochemical Co., Ltd. Maltose (Mal) was obtained from Sigma. Fructose (Fru) was purchased from Tianjin Zonghengxing Industry and Trade Co., Ltd. Chemical Reagent Branch. Sucrose (Suc) was obtained from Tianjin Taixing Chemical Co., Ltd. Glycine (Gly) was obtained from Tianjin Dongfang Sanitary Materials Factory. Calcium chloride ($CaCl_2$) and hydrochloric acid (HCl) were purchased from Tianjin Damao Chemical Reagent Factory. Anhydrous sodium sulfate (Na_2SO_4) was obtained from Tianjin Tianda Chemical Experimental Factory. Potassium chloride (KCl) and sodium hydroxide (NaOH) were purchased from Tianjin Standard Technology Co., Ltd. Histidine (His) and lysine (Lys) were obtained from Beijing Solarbio Science & Technology Co., Ltd.

Instruments

Transmission electron microscopy (TEM) images were obtained using a Tecnai G2 F20 S-TWIN TEM (FEI, USA). Fourier transform infrared spectroscopy (FT-IR) was performed to analyze the functional groups of the materials on a Thermo Nicolet iS10 Fourier transform infrared spectrometer (Thermo Fisher Scientific, USA). The water contact angle of the test strips was measured by the sessile drop method using an optical contact angle meter (OCA 15EC, Dataphysics, Germany). The elemental composition and chemical states were investigated using an X-ray photoelectron spectrometer (XPS, ESCALAB Xi+, Thermo Fisher Scientific, USA). The pH of the solutions was adjusted using a LeiCi PHS-3E pH meter. UV-visible absorption spectra were recorded on a UV-2600 spectrophotometer (Techcomp, China). Fluorescence intensity was measured using a fluorescence spectrophotometer (F-7100, Hitachi High-Technologies, Japan), and fluorescence lifetime was determined using a fluorescence spectrometer (FS5, Edinburgh Instruments Ltd, UK).

Synthesis of Fe(II)/silane-derived carbon dots (Fe(II)/CDs)

The following procedure was slightly modified based on previous literature [16]. Briefly, 1.5 mL of APTMS was added to 10 mL of glycerol, followed by degassing with nitrogen for 2 min. After heat treatment at 260 °C for 12 hours, the cooled solid residue was added to 20 mL of deionized water. The CD solution was collected by centrifugation at 8000 rpm for 10 minutes, and then purified using a dialysis membrane (molecular weight cutoff: ~1 kDa) for 24 hours. Finally, the CDs were freeze-dried to obtain a brown oily substance (~10 mg), which was stored at room temperature for later use.

Subsequently, 1 mL of CDs (10 mg/mL) was mixed with 1 mL of 1.4 mM $FeSO_4$ solution to obtain Fe(II)/CDs (pH = 2.6).

The portable dual-readout paper-based sensor for the detection of glucose

To develop a portable dual-readout paper-based glucose sensor, eco-friendly and biodegradable rosin was used as the material to fabricate the hydrophobic barrier. The specific procedures are as follows: First, a rosin ethanol solution (0.25 g/mL) was prepared and uniformly coated on both sides of the filter paper. Meanwhile, the rosin ethanol solution was loaded into a refillable bio-ink pen to ensure precise application. Next, a 2 mm-wide hydrophobic boundary was uniformly drawn around the edge of the circular detection area using a nylon gasket with a diameter of 10 mm.

The detection procedures of the sensor were as follows: Glu solutions with different concentrations were incubated with GOx at 37 °C for 30 min (pH = 5.7). Colorimetric readout mode (CRM): After adding 10 μL of the incubated glucose solutions with different concentrations to the detection zone, 10 μL of Fe(II)/CDs, 5 μL of TMB (5.5 mM), and 75 μL of deionized water were added sequentially, followed by incubation for 20 min. A Python-based RGB image analysis algorithm was applied to analyze the images. Fluorescence readout mode (FRM): TMB was omitted and the volume of deionized water was increased to 80 μL to maintain a total assay volume of 100 μL; all other procedures were identical to those used for CRM. Photographs were taken using a smartphone (vivo X60) in an ultraviolet (UV) light box. To evaluate potential interference, the effects of Mal, Suc,

Fru, Na^+, Ca^{2+}, K^+, and SO_4^{2-} on the B/(R+G+B) values of the Fe(II)/CDs system in both FRM and CRM were assessed using the same procedure.

Image acquisition and RGB analysis

Fluorescence and colorimetric images of the paper-based sensor were captured using a smartphone under fixed imaging conditions. During image acquisition, the camera sensitivity was set to ISO 2000, and the autofocus fine-adjustment compensation value was set to 0. The shooting distance, camera angle, illumination conditions, and other imaging parameters were maintained consistently throughout the experiments to minimize image-to-image variation.

Before RGB analysis, each photograph was manually cropped along the boundary of the 10-mm-diameter detection zone to exclude the surrounding paper and background. The same cropping criterion was applied to all images. No automatic detection-zone localization or image segmentation was performed. The cropped images were subsequently imported into a Python-based image-processing program, which automatically calculated the mean red (R), green (G), and blue (B) channel values of all pixels within the cropped region. The normalized blue-channel parameter, (B/(R+G+B)), was used as the quantitative analytical signal to reduce the influence of variations in overall image brightness. The relationship between (B/(R+G+B)) and glucose concentration was then established for the fluorescence and colorimetric readout modes. The algorithm code was provided in Table S1.

Instrument-assisted validation of glucose detection

To verify the accuracy of the sensor, ultraviolet-visible (UV-Vis) spectrophotometry and fluorescence spectrophotometry were used for auxiliary detection. UV-Vis Spectrophotometry: 50 μL of GOx (1 mg/mL) was incubated with 50 μL of Glu (pH = 5.7) at 37 ℃ for 30 min. Subsequently, 100 μL of Fe(II)/CDs, 50 μL of 5.5 mM TMB, and 750 μL of deionized water were added, followed by incubation for 20 min. The absorption signal at 652 nm was then measured using UV-Vis spectrophotometry. Fluorescence spectrophotometry: The procedure was the same as that used for UV-Vis spectrophotometry, except that TMB was omitted and the volume of deionized water was increased to 800 μL to maintain a total assay volume of 1 mL and the fluorescence intensity was

recorded. To evaluate potential interference, the effects of Mal, Suc, Fru, Na^+, Ca^{2+}, K^+, and SO_4^{2-} on the fluorescence intensity and UV-Vis absorption intensity of the Fe(II)/CDs system were assessed using the same procedure.

Real sample detection

To evaluate the practical applicability of the developed method, glucose detection was performed in human serum. Human blood samples were collected from the Affiliated Hospital of Hebei University following approval by the Ethics Committee of the Affiliated Hospital of Hebei University (Approval No. HDFYLL-IIT-2026-011). Written informed consent was obtained from all participants or, where applicable, from their legal guardians prior to sample collection. All experiments were conducted in accordance with the relevant laws and institutional guidelines of the university. The whole blood samples were allowed to stand at room temperature for 2 h, followed by centrifugation at 3000 rpm for 15 min at room temperature to collect the supernatant. The obtained supernatant was diluted 10-fold to prepare human serum samples, which were stored at 4 °C for further use. Finally, the pretreated human serum samples were spiked with glucose at different concentrations, and the spiked samples were detected using the same procedure as the glucose detection analysis described above.

Results and discussion

Synthesis and characterisation of Fe(II)/CDs

The TEM image (Fig. 1a) and the corresponding size distribution histogram (Fig. 1b) showed that the Fe(II)/CDs had an average size of ~3.35 nm with a spherical shape. As shown in Fig. 1c, the UV-Vis absorption spectrum of Fe(II)/CDs exhibited a strong absorption band at 270 nm, which was attributed to the π-π* transition of aromatic C=C bonds. In contrast, two broad absorption bands at ~300 nm and ~345 nm were assigned to the n-π* transition of C=O bonds [24–26]. In addition, Fe(II)/CDs displayed a characteristic fluorescence emission peak at 430 nm, and three distinct excitation peaks were observed at 240 nm, 300 nm, and 350 nm (In this work, 350 nm was used as the excitation wavelength). As shown in Fig. 1d and 1e, the fluorescence intensity of

Fe(II)/CDs changed slightly when the pH value increased from 2 to 8 and the ionic strength varied from 0 to 1 M (NaCl solution), indicating that it could maintain good optical stability under different environmental conditions.

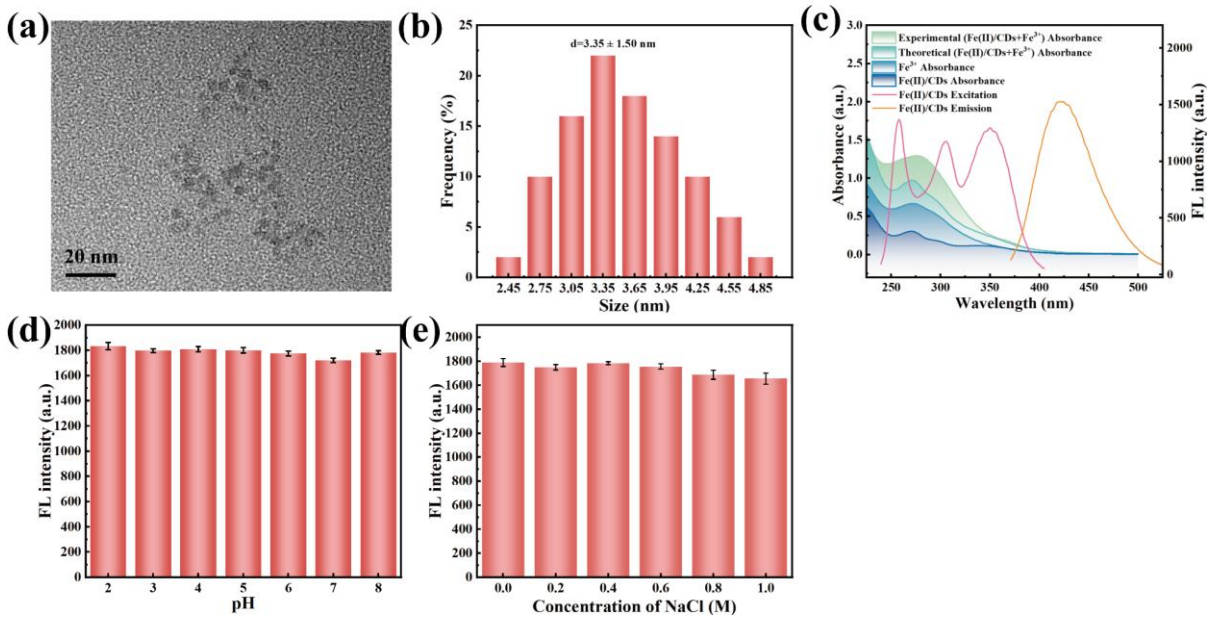


Fig. 1 (a) TEM image of Fe(II)/CDs, (b) Particle size distribution histogram of Fe(II)/CDs, (c) UV-Vis absorption of Fe(II)/CDs, Fe^{3+} (100 μM), and Fe(II)/CDs + Fe^{3+} (the experimental curve and theoretical curve), fluorescence excitation and emission spectra of Fe(II)/CDs. The theoretical curve was obtained by the physical addition of the spectrum of Fe(II)/CDs solution and Fe^{3+} solution. (d) Fluorescence intensity under different pH values, (e) Fluorescence intensity under different salt concentrations

Feasibility and mechanism analysis of the dual-readout glucose detection

The optimal reaction conditions for glucose oxidation were determined as pH 5.7 and 30 min incubation. The Fenton reaction exhibits a high hydroxyl radicals (·OH)-generation rate within the pH range of 2.7–3.5 [27,21]. However, some commonly used buffer components can coordinate with Fe^{3+}, thereby altering iron speciation and potentially affecting Fenton reaction kinetics. Therefore, no buffer was used to directly regulate the pH of the reaction mixture. Instead, the acidity of the final reaction system was controlled by adjusting the initial pH of the Fe(II)/CDs solution. When the initial pH values of the Fe(II)/CDs solution were adjusted to 2.2, 2.4, 2.6, 2.8, and 3.0, the corresponding final pH values of the reaction mixtures were 3.16, 3.33, 3.48, 3.69, and 3.88, respectively.

The initial pH of the Fe(II)/CDs solution was further optimized. As shown in Fig. S1, the colorimetric response (A/A_0) increased with the initial pH of the Fe(II)/CDs solution and reached a maximum at pH 2.6. In contrast, the fluorescence response exhibited a different pH (the initial pH of the Fe(II)/CDs solution: 2.2-3.0) dependence. Considering the strong colorimetric response and the requirement for a unified reaction condition for both readout modes, an initial Fe(II)/CDs pH of 2.6 was selected for subsequent dual-readout experiments. As shown in Fig. 2a, the increase in glucose concentration caused significant fluorescence quenching of the Fe(II)/CDs system, while Fig. 2b showed that the absorbance peak at 652 nm increased significantly with the rise of glucose concentration, indicating that both fluorescence and colorimetric methods could be used for quantitative detection of glucose. The fluorescence quenching and absorbance enhancement observed in the Fe(II)/CDs system were attributed to H_2O_2 produced during the glucose oxidase (GOx)-catalyzed oxidation of glucose. The resulting H_2O_2 initiated the Fenton reaction, during which Fe^{2+} was oxidized to Fe^{3+}. The generated Fe^{3+} subsequently quenched the fluorescence of the Fe(II)/CDs. Meanwhile, Fe^{3+} and ·OH produced during the Fenton reaction promoted the oxidation of colorless 3,3′,5,5′-tetramethylbenzidine (TMB) into its blue oxidized form (oxTMB) [28,29], thereby increasing the absorbance of the system. To further clarify the role of CDs in the colorimetric readout mode, the TMB oxidation activities of different reaction systems were compared. As shown in Fig. 2c, the Fe(II)/CDs + H_2O_2 + TMB system exhibited a stronger absorbance response than the Fe^{2+} + H_2O_2 + TMB system, whereas CDs + H_2O_2 + TMB produced only a weak response. These results suggested that the interaction between Fe^{3+} and the surface functional groups of the CDs might facilitate H_2O_2 activation and enhance oxidation of TMB [18].

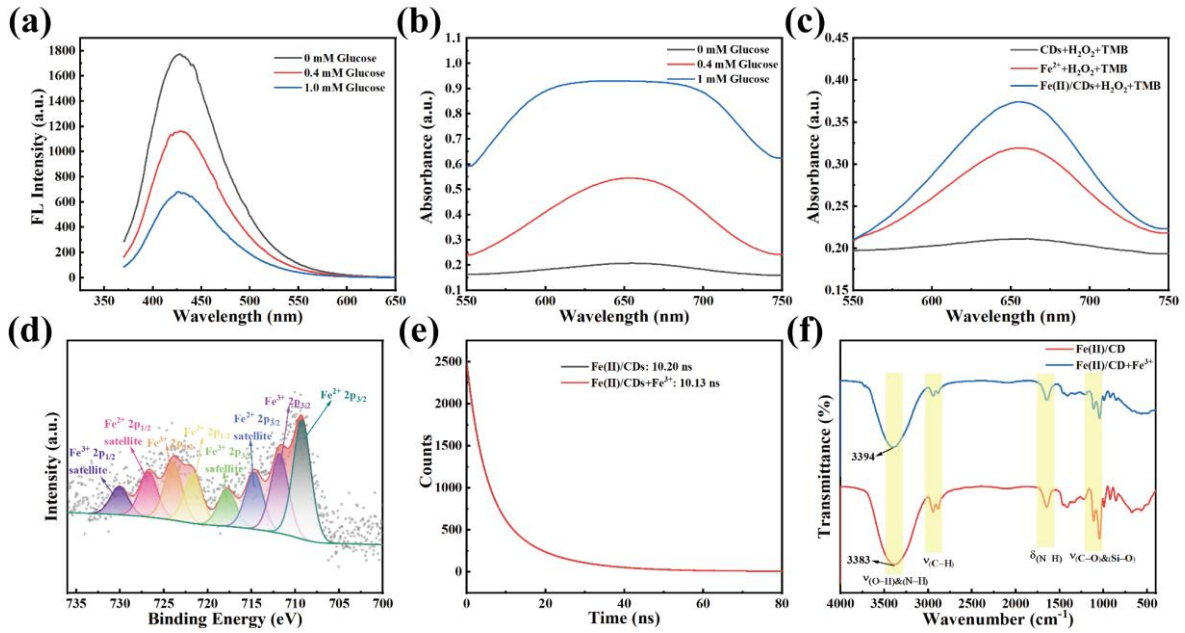


Fig. 2 (a) Feasibility analysis of the fluorescence response, (b) feasibility analysis of the colorimetric response, (c) Absorbance responses at 652 nm of CDs + H_2O_2 + TMB, Fe^{2+} + H_2O_2 + TMB, and Fe(II)/CDs + H_2O_2 + TMB systems. (d) high-resolution XPS spectrum of Fe 2p of the Fe(II)/CDs fluorescence probe after H_2O_2 addition, (e) time-resolved fluorescence decay spectra of Fe(II)/CDs system before and after the addition of Fe^{3+}, respectively, (f) FTIR spectrum of Fe(II)/CDs system with Fe^{3+} addition

To further investigate the glucose detection mechanism, both Fe^{2+} and Fe^{3+} signals were observed in the XPS spectrum of the Fe(II)/CDs fluorescence probe after H_2O_2 addition [30–32], confirming the occurrence of the Fenton reaction(Fig. S2 and Fig. 2d). To elaborate on the underlying mechanism of fluorescence quenching, the fluorescence lifetimes of two distinct systems were measured independently: Fe(II)/CDs alone, Fe(II)/CDs in the presence of Fe^{3+} (Fig. 2e). The results revealed negligible differences in fluorescence lifetimes between the Fe(II)/CDs alone and Fe(II)/CDs with Fe^{3+} systems, indicating that the quenching process did not involve dynamic collision or fluorescence resonance energy transfer (FRET). Fig. 1c showed that the experimental curve (the absorption spectrum of Fe(II)/CDs + Fe^{3+}) did not coincide with the theoretical curve (the physical addition of the spectra of Fe(II)/CDs solution and Fe^{3+} solution), indicating the formation of stable metal ion-CDs complexes. Additionally, the fluorescence excitation spectrum of Fe(II)/CDs exhibited no overlap with the UV–vis absorption spectrum of Fe^{3+}, confirming that the fluorescence quenching could not be attributed to internal filtering effects (IFE). Meanwhile, the FTIR spectra of Fe(II)/CDs and Fe(II)/CDs+ Fe^{3+} were compared (Fig. 2f).

The results showed that the O-H/N-H stretching vibration blue-shifted after Fe^{3+} addition, indicating the formation of a non-fluorescence complex, which belongs to static quenching. Specifically, Fe^{3+} may coordinate or form complexes with amino and/or oxygen-containing functional groups on the surface of the carbon dots. This was consistent with previous reports in the literature [17]. The detection mechanism is illustrated in Fig. 3.

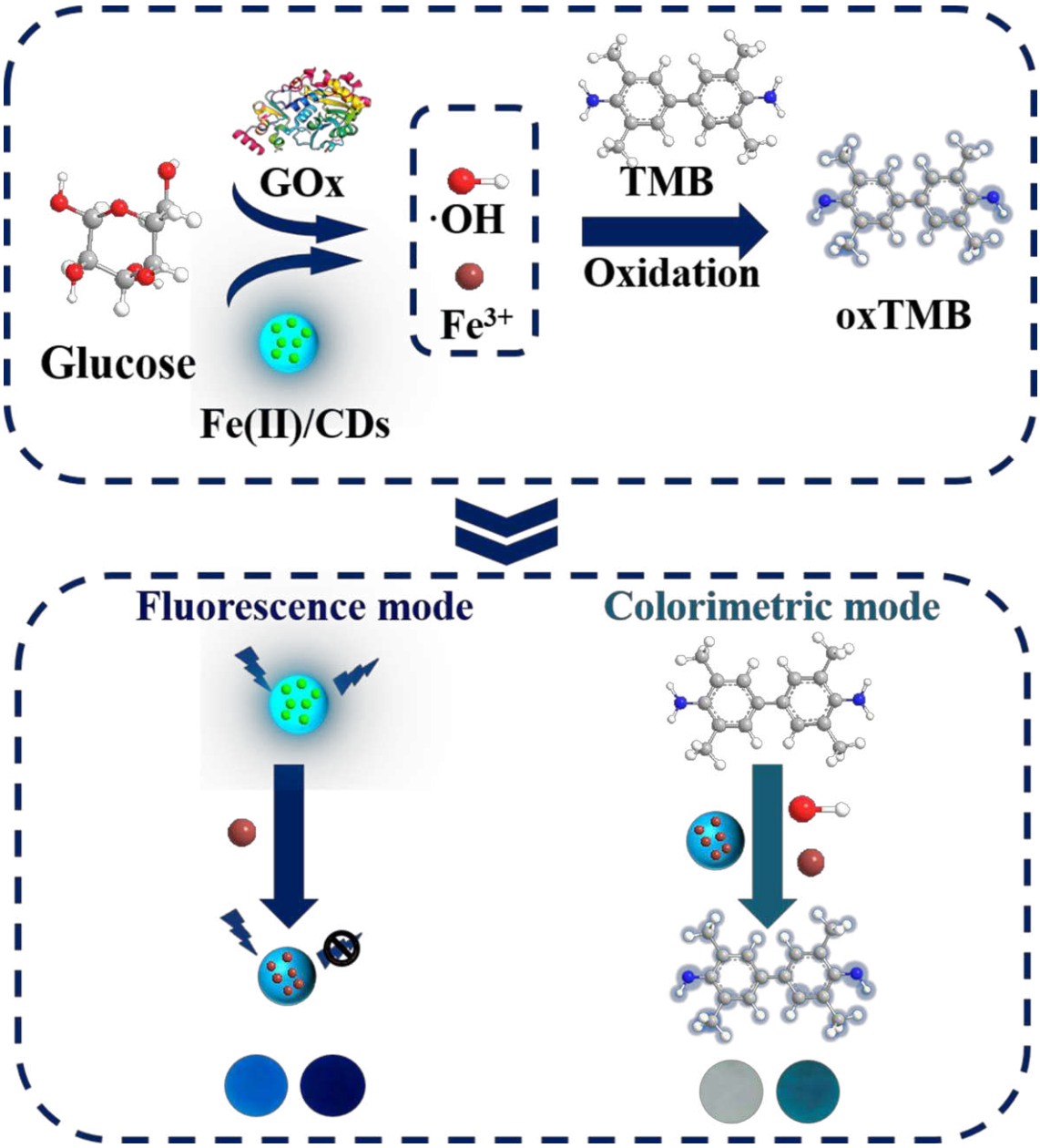


Fig. 3 Mechanism diagram of fluorescence/colorimetric glucose detection based on Fe(II)/CDs

Performance of the portable dual-readout glucose paper-based sensor

A portable dual-readout paper-based sensor for on-site glucose detection was developed by leveraging the Fenton reaction between Fe(II)/CDs and H_2O_2. In sensor design, the establishment of an effective hydrophobic boundary was crucial to confine the test solution within the detection area. Experimental results showed that the rosin-coated area exhibited excellent hydrophobic properties, with a contact angle of 98° after 30 s of droplet deposition (Fig. S3), which effectively prevented liquid diffusion. As shown in Fig. 4a–4c, the reaction time, initial $FeSO_4$ concentration, and TMB concentration were systematically optimized. Both readout modes reached relatively stable responses after 20 min. The fluorescence response was optimal at an initial $FeSO_4$ concentration of approximately 1.2 mM, whereas the colorimetric response reached its maximum at approximately 1.4 mM. Considering the requirement for a unified operating condition for the dual-readout platform, 1.4 mM $FeSO_4$ was selected for subsequent experiments. In CRM, 5.5 mM TMB was selected as the optimal concentration based on the plateau in absorbance response. Subsequent experiments were carried out under these optimized conditions. A smartphone was used to rapidly capture the image-derived readout signals obtained from the fluorescence readout mode (FRM) and colorimetric readout mode (CRM), and a Python-based RGB extraction algorithm was then employed to accurately calculate the B/(R+G+B) mean values, thereby establishing a linear relationship with glucose concentration. As the glucose concentration increased, the G- and B-channel values showed overall decreasing trends, whereas the R-channel values remained relatively low and exhibited minor fluctuations (Table S2). Meanwhile, the total RGB signal (R+G+B) decreased, indicating an overall attenuation of the recorded fluorescence image. Because the relative decrease in the G channel was greater than that in the B channel, the proportion of the B-channel signal in the total RGB signal increased despite the decrease in its absolute value. Therefore, B/(R+G+B) represents a normalized blue-channel fraction rather than the absolute blue fluorescence intensity. As shown in Fig. 4d-4f, B/(R+G+B) image parameter in FRM showed a good linear relationship with glucose concentration over the range of 0.01–1.00 mM under UV excitation and was therefore used for smartphone-based quantitative analysis. As shown in Fig. 4f, the linear regression equation for glucose concentration in the range of 0.01–1 mM was $Y = 0.5961 + 0.0497X$ ($R^2 = 0.998$), and the limit of detection (LOD) was calculated to be 2.9 μM based on $3\sigma/S$ (where σ was the standard deviation of 11 blank samples, and S was the slope of the calibration curve), and the limit of quantitation (LOQ) was 9.7 μM based on $10\sigma/S$. Meanwhile, the detailed R, G, and B channel values for CRM were provided in Table S3. Similar to the FRM results, the increase

in B/(R+G+B) primarily reflected an increased relative contribution of the blue channel to the total RGB signal, rather than an increase in the absolute B-channel intensity. As shown in Fig. 4g–4i, the blue color in CRM gradually deepened with increasing glucose concentration due to the enhanced formation of oxTMB. The corresponding linear regression equation in the range of 0.01–1 mM was Y = 0.3192 + 0.2163X (R^2 = 0.995), with LOD of 2.5 μM and LOQ of 8.3 μM. Compared with the references listed in Table S4, the Fe(II)/CDs nanocomposite exhibited a relatively wide linear range and low LOD. The estimated material cost was approximately 1.58 RMB per filter paper containing 16 assay zones, corresponding to approximately 0.10 RMB per assay zone(Table S5).

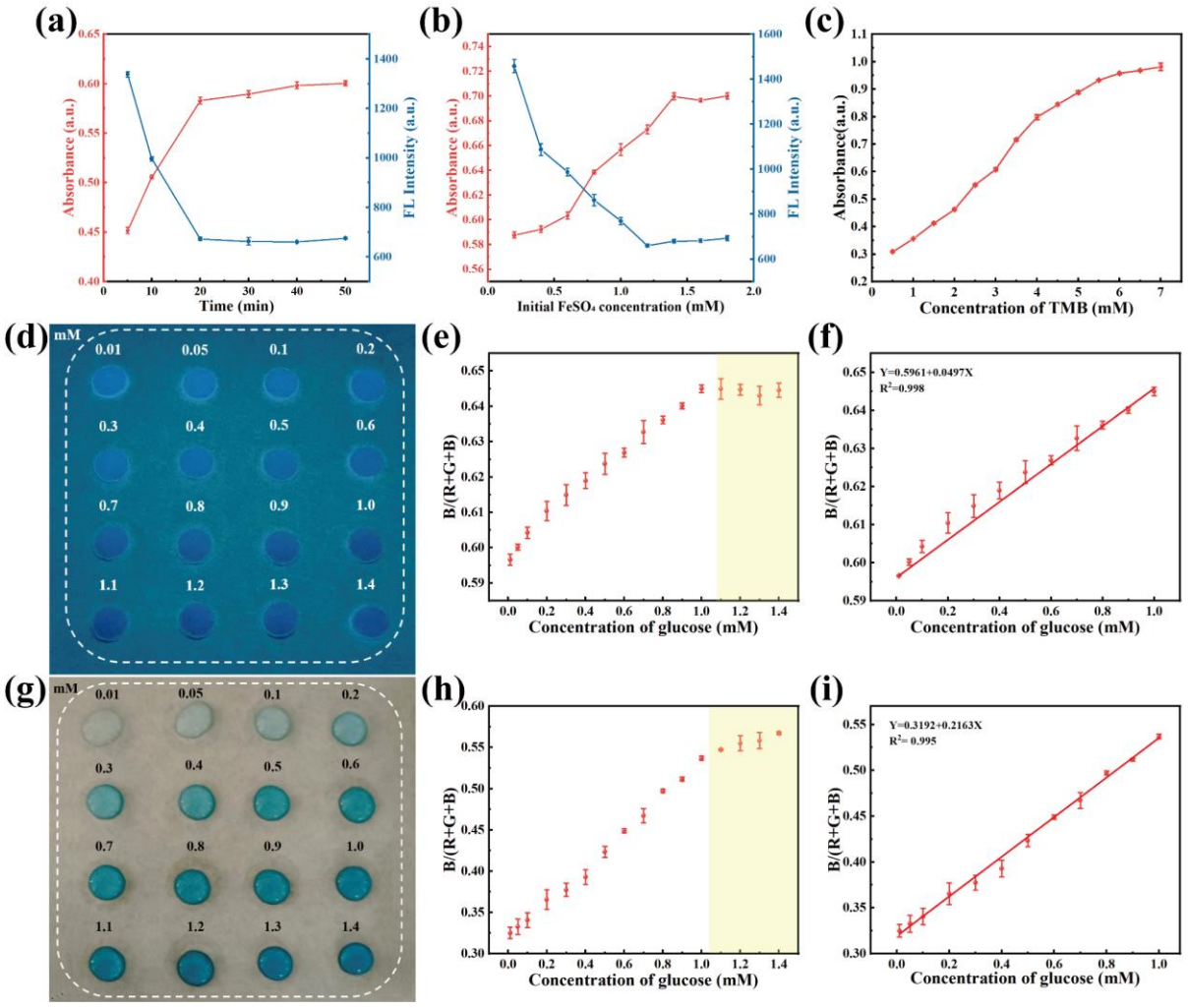


Fig. 4 Optimization of experimental parameters of FRM and CRM: (a) Reaction time, (b) Initial $FeSO_4$ concentration (mM), (c) Optimal concentration of TMB. Image-derived readout signals of glucose at different concentrations obtained using the

paper-based sensor: (d) FRM images, (e–f) B/(R+G+B)-based calibration plots in FRM, (g) CRM images, and (h–i) B/(R+G+B)-based calibration plots in CRM

The applicability and user-friendliness of the sensor were significantly improved, which could meet diverse detection requirements. The accuracy of the sensor was further verified by using a spectrophotometer as an auxiliary detection method (Fig. S4).

Selectivity investigations of the sensor

To evaluate the selectivity and anti-interference capability of the proposed sensor, common sugars, inorganic ions, amino acids, and endogenous redox-active species were investigated. As shown in Fig. 5a and 5b, Mal, Suc, Fru, Na^{+}, Ca^{2+}, K^{+} and SO_4^{2-}, Gly, and Lys caused only limited variations in the responses of both FRM and CRM in the presence of glucose, indicating good tolerance toward these coexisting species. Instrumental measurements further confirmed the overall trends observed from smartphone-based analysis (Fig. S5). In contrast, AA, UA, and His all interfered with the sensing response, with AA showing the most pronounced effect. This behavior was likely associated with the redox activity of AA and UA and the possible interaction of His with iron species, which may perturb Fe(II)/Fe(III) cycling and the subsequent Fenton-mediated optical responses[33]. Overall, the proposed sensor exhibited satisfactory anti-interference capability toward most tested coexisting substances, although redox-active interferents should be considered in complex biological samples.

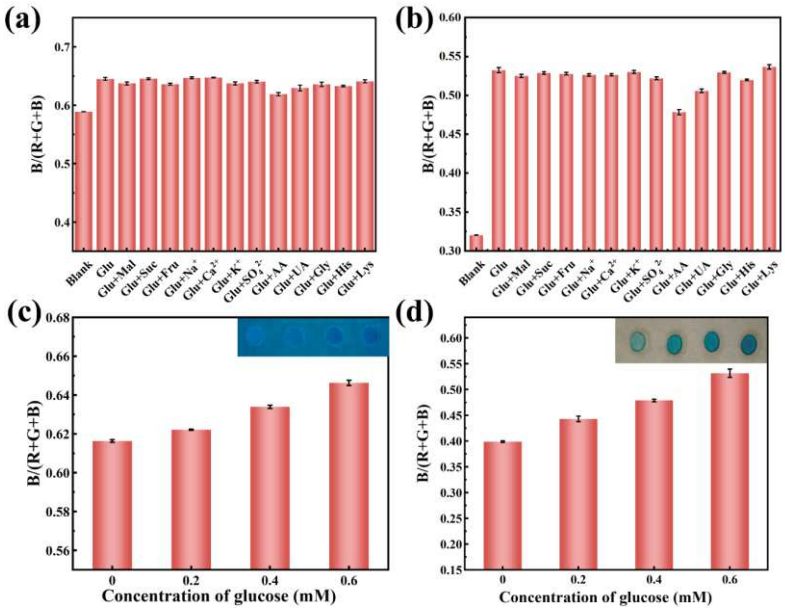


Fig. 5 Selectivity and anti-interference performance of the paper-based sensor for glucose detection: (a) FRM, (b) CRM, with glucose concentration of 1 mM and interference concentration of 1 mM. Glucose detection in real samples: (c) FRM; (d) CRM

Practical applications

To evaluate its practical applicability, the developed paper-based sensor was applied to glucose determination in human serum through spike-recovery experiments. The serum was pretreated as described in Real sample detection section and diluted tenfold prior to analysis. The endogenous glucose concentrations in the diluted serum were determined to be 0.40 mM using the fluorescence readout mode (FRM) and 0.36 mM using the colorimetric readout mode (CRM), and these values were used as the corresponding baseline concentrations for the recovery calculations. After glucose was added at concentrations of 0.2, 0.4, and 0.6 mM, the recoveries obtained using FRM and CRM were 90.00–91.67% and 95.00–105.00%, with relative standard deviations (RSD) not exceeding 3.40% and 4.29%, respectively (Table 1, Fig. 5c and 5d). Moreover, the glucose concentrations determined using the paper-based sensor were in close agreement with those obtained by fluorescence spectrophotometry and UV–Vis spectrophotometry (Fig. S6). These results demonstrate the satisfactory accuracy and precision of the proposed sensor in diluted human serum and support its proof-of-concept applicability to portable glucose analysis in complex biological matrices.

Table 1 Determination of glucose in spiked human serum using the paper-based sensor and instrumental methods.

Samples	Added (mM)	FRM[a]			CRM[b]			Large-scale instrument	
		Found (mM, *n* =3)	Recovery (%)	RSD (%)	Found (mM, *n* =3)	Recovery (%)	RSD (%)	FL (mM)	UV-vis (mM)
1	0	0.40	-	3.40	0.36	-	1.91	0.38	0.36
2	0.2	0.58	90.00	0.99	0.57	105.00	4.29	0.57	0.53
3	0.4	0.76	90.00	2.23	0.74	95.00	1.58	0.77	0.74
4	0.6	0.95	91.67	2.85	0.98	103.33	3.74	0.96	0.96

[a] FRM: fluorescence readout mode; [b] CRM: colorimetric readout mode

Conclusions

In this study, a dual-mode paper-based sensor based on Fe(II)/silane-derived carbon dot system (Fe(II)/CDs) was developed for the fluorescence–colorimetric detection of glucose. In this sensing system, glucose was catalyzed by glucose oxidase to produce H_2O_2, which subsequently triggered the Fe(II)/CDs-mediated Fenton reaction, thereby enabling a fluorescence–colorimetric dual-signal response. In addition, a portable paper-based sensing platform was fabricated using biodegradable rosin as the hydrophobic zone. By integrating smartphone image acquisition with a Python-based RGB analysis algorithm, quantitative detection of glucose was achieved without the need for large-scale instruments. Under optimized conditions, the limits of detection of the sensor were 2.9 μM and 2.5 μM in FRM and CRM, respectively, with corresponding LOQs of 9.7 μM and 8.3 μM. The detection results in spiked serum samples demonstrated the satisfactory accuracy and reliability of this method. Overall, these results demonstrate the feasibility of the proposed platform for smartphone-assisted glucose determination and its potential for low cost, portable and on-site analysis.

Appendix A. Supplementary data

Supplementary data related to this article can be found at XXX

Acknowledgments

This work was financially supported by Natural Science Foundation of Hebei Province (B2025205014), Hebei Province Higher Education Scientific Research Project (JCZX2025005), Hebei Normal University Science and Technology Fund Project (L2025B54, L2026B11), Hebei University Graduate Student University-Level Innovation Capability Cultivation Funding Project (HBU2026BS007), and Hebei University College Student Innovation and Entrepreneurship Training Program Project (DC2026288).

CRediT authorship contribution statement

L-L.D.: Conceptualization, Data curation, Formal analysis, Software, Writing – original draft preparation. **C-Q.Z.:** Data curation, Investigation. **Y-F.D.:** Investigation, Validation. **M-X.H.:** Methodology. **Z-G.W.:** Funding acquisition, Writing – review & editing. **L-Q.Y.:** Supervision, Project administration. **Y-K.L.:** Formal analysis, Supervision, Writing – review & editing.

Data availability

No datasets were generated or analysed during the current study.

Declarations

Ethical approval All experiments involving samples were approved by the Ethics Committee of the Affiliated Hospital of Hebei University (Approval No. HDFYLL-IIT-2026-011). The name of the Approval Committee: Ethics Committee of the Affiliated Hospital of Hebei University.

Consent to participate All human blood samples used in this study were obtained with written informed consent from all participants.

Competing Interest All the authors declare no competing financial interest.

Clinical trial number Not applicable.

Disclosure about using AI tools

It is declared that no AI tools were used for preparation of this manuscript, including figures and Graphical Abstract.

References

1. A.K., B.; Niharika, D.G.; Murthy, C.K.; Raju, K.S.; Salaria, P.; M., A.R. Smart nanoprobes in diabetes management: Emerging role of carbon quantum dots in diagnosis and therapy. Sens. Actuators A: Phys., 2026, 400, 117490. https://doi.org/10.1016/j.sna.2026.117490
2. Zhao, L.; Yuan, J.; Yang, Q.; Ma, J.; Yang, F.; Zou, Y.; Liu, K.; Liu, F. Diabetes and its complications: molecular mechanisms, prevention and treatment. Sig Transduct Target Ther, 2026, 11, 22. https://doi.org/10.1038/s41392-025-02401-w
3. Kushner, P.R.; Fonseca, V.; Nichols, J.H.; Shubrook, J.H.; Miller, E.; Wright, E.; DeFilippi, C.; Vassalotti, J.A. Clinical Need for Point-of-Care Testing for Diabetes in Clinical and Laboratory Improvement Amendments–Waived Settings. Clinical Diabetes, 2024, cd240071. https://doi.org/10.2337/cd24-0071
4. Drain, P.K. Point-of-Care Diagnostics (POCD) in Resource-Limited Settings. Diagnostics, 2024, 14, 1926. https://doi.org/10.3390/diagnostics14171926
5. Yang, X.; Duan, X.; Zhu, L.; Zhao, X.; Zhang, S.; Ni, S.; Wu, S.; Han, Z.; Sun, D.; Deng, W.; Chen, Q.; Wu, W. Carbon dots assemblies with zinc as activable fluorescence probe for local glucose monitoring in traumatic wounds. Talanta, 2026, 296, 128512. https://doi.org/10.1016/j.talanta.2025.128512
6. Cirillo, C.; Iuliano, M.; Sarno, M. $ZnFe_2O_4$/GQDs Nanoparticles as Peroxidase Mimics for Sensitive and Selective Colorimetric Detection of Glucose in Real Samples. Micromachines, 2025, 16, 520. https://doi.org/10.3390/mi16050520
7. Cebrián, P.; Pérez-Sienes, L.; Sanz-Vicente, I.; López-Molinero, Á.; De Marcos, S.; Galbán, J. Solving Color Reproducibility between Digital Devices: A Robust Approach of Smartphones Color Management for Chemical (Bio)Sensors. Biosensors, 2022, 12, 341. https://doi.org/10.3390/bios12050341
8. Yang, F.; Liu, D.; Lin, H.; Zhang, H.; Zhang, P.; Li, C.; Dong, J.; An, S.; Ren, F.; Ge, X.; Cheng, L.; Wang, F.; Liu, T.; Liu, J.; Fu, J.; Tang, F.; Pan, H.; Zou, L.; Ma, X.; Ma, H.; Rong, S. Innovative dual-mode colorimetric/fluorescent sensors based on transition metal nanozymes: mechanisms, applications, and future perspectives. Microchim Acta, 2026, 193, 265. https://doi.org/10.1007/s00604-026-07931-w
9. Al Lawati, H.A.J.; Hassanzadeh, J. Dual-function 2D cobalt metal-organic framework embedded on paper as a point-of-care diagnostic device: Application for the quantification of glucose. Anal. Chim. Acta, 2020, 1139, 15–26. https://doi.org/10.1016/j.aca.2020.09.026

10. Chen, Z.; Zhang, Y.; Teng, R.; Li, M.; Ding, C.; Huang, Y. AIE multifunctional probe empowering colorimetric-fluorescence dual-mode biosensor for early diabetic screening. Biosens. Bioelectron., 2025, 269, 116941. https://doi.org/10.1016/j.bios.2024.116941
11. Ngo, Y.-L.T.; Nguyen, P.L.; Jana, J.; Choi, W.M.; Chung, J.S.; Hur, S.H. Simple paper-based colorimetric and fluorescent glucose sensor using N-doped carbon dots and metal oxide hybrid structures. Anal. Chim. Acta, 2021, 1147, 187–198. https://doi.org/10.1016/j.aca.2020.11.023
12. Wang, L.; Zheng, S.; Lu, L.; Li, C.; Wang, F. A dual-mode ratiometric fluorescence and smartphone-assisted colorimetric sensing platform based on bifunctional Fe,Co-CQD for glucose analysis at physiological pH. Analytica Chimica Acta, 2023, 1239, 340701. https://doi.org/10.1016/j.aca.2022.340701
13. Parcheforosh, A.; Khodaei Tehrani, A.; Habibi, A.; Taghipour, F. UV-activated biosensor based on molecularly imprinted polymer and carbon quantum dots for lactate measurement. Analytica Chimica Acta, 2026, 1399, 345299. https://doi.org/10.1016/j.aca.2026.345299
14. Fu, Q.; Zhou, X.; Wang, M.; Su, X. Nanozyme-based sensitive ratiometric fluorescence detection platform for glucose. Analytica Chimica Acta, 2022, 1216, 339993. https://doi.org/10.1016/j.aca.2022.339993
15. Chatzimitakos, T.G.; Kasouni, A.I.; Stalikas, C.D. Multi-purpose nitrogen and phosphorous codoped carbon nanodots for fluorescence-based sensing and bioimaging. Chemical Engineering Journal, 2023, 476, 146686. https://doi.org/10.1016/j.cej.2023.146686
16. Gao, G.; Jiang, Y.-W.; Yang, J.; Wu, F.-G. Mitochondria-targetable carbon quantum dots for differentiating cancerous cells from normal cells. Nanoscale, 2017, 9, 18368–18378. https://doi.org/10.1039/C7NR06764J
17. Gao, G.; Jiang, Y.-W.; Jia, H.-R.; Yang, J.; Wu, F.-G. On-off-on fluorescent nanosensor for Fe^{3+} detection and cancer/normal cell differentiation via silicon-doped carbon quantum dots. Carbon, 2018, 134, 232–243. https://doi.org/10.1016/j.carbon.2018.02.063
18. Li, J.; Hu, Z.-E.; We, Y.-J.; Liu, Y.-H.; Wang, N.; Yu, X.-Q. Multifunctional carbon quantum dots as a theranostic nanomedicine for fluorescence imaging-guided glutathione depletion to improve chemodynamic therapy. J. Colloid Interface Sci., 2022, 606, 1219–1228. https://doi.org/10.1016/j.jcis.2021.08.114
19. Liao, Z.; Zhong, J.; Tang, X.; Peng, Z.; Xu, P.; Qiu, P. Smartphone-assisted portable swabs for blood glucose management: A point-of-use assay for dual-mode visual detection based on bifunctional carbon dots. Talanta, 2024, 278, 126545. https://doi.org/10.1016/j.talanta.2024.126545
20. Roller, R.M.; Lieberman, M. Beyond wax printing: The future of paper analytical device fabrication. Sensors and Actuators B: Chemical, 2023, 392, 134059. https://doi.org/10.1016/j.snb.2023.134059
21. Wang, Z.; Du, Y.; Zhou, P.; Xiong, Z.; He, C.; Liu, Y.; Zhang, H.; Yao, G.; Lai, B. Strategies based on electron donors to accelerate Fe(III)/Fe(II) cycle in Fenton or Fenton-like processes. Chemical Engineering Journal, 2023, 454, 140096. https://doi.org/10.1016/j.cej.2022.140096
22. Li, J.; Li, Y.; Shi, Y.; Li, Z.; Deng, C.; Zhang, G.; Zhou, Q.; Wang, Z.; Yu, X. Fluorescence/colorimetric intelligent sensor based on Fe-adsorbing carbon dots nanozymes for selective recognition and quantification of total antioxidant capacity in foods and cells. Food Chemistry, 2025, 490, 145052. https://doi.org/10.1016/j.foodchem.2025.145052
23. Wu, S.; Yu, Z.; Zhao, J.; Wang, Y.; Nan, J.; Xu, L.; Li, X.; Yang, L.; Dong, S. Fluorescent Nanozyme Based on Bimetallic Fe/Co-Doped Carbon Dots for Dual-Mode Detection of Ascorbic Acid and Hydrogen Peroxide. Anal. Chem., 2025, 97, 15320–15328. https://doi.org/10.1021/acs.analchem.5c02107

24. Mehrabi, F.; Hosseini, M.; Sadeghi, N.; Mohammadi, J.; Ganjali, M.R.; Ranjbar, B. Green emitting carbon dots-immunosensor on magnetic nanoparticles for detection of Nanog antigen as a cancer stem cell biomarker. Analytica Chimica Acta, 2025, 1353, 343960. https://doi.org/10.1016/j.aca.2025.343960
25. Li, Y.; Zhang, X.; Lu, Q.; Cao, J.; Gao, S.; Liu, Q.; Cai, X.; Zhao, H. Cellulose-based yellow-green emitting carbon dots with large Stokes shift as effective "turn off-on" fluorescence platforms for Cr(VI) and AA dual efficacy detection. Analytica Chimica Acta, 2024, 1324, 343102. https://doi.org/10.1016/j.aca.2024.343102
26. Rodríguez-Varillas, S.; Fontanil, T.; Espina Casado, J.; Fernández-González, A.; Badía Laíño, R. Surface modification of carbon dots with cyclodextrins as potential biocompatible photoluminescent delivery/bioimaging nanoplatform. Analytica Chimica Acta, 2024, 1318, 342948. https://doi.org/10.1016/j.aca.2024.342948
27. Fischbacher, A.; Von Sonntag, C.; Schmidt, T.C. Hydroxyl radical yields in the Fenton process under various pH, ligand concentrations and hydrogen peroxide/Fe(II) ratios. Chemosphere, 2017, 182, 738–744. https://doi.org/10.1016/j.chemosphere.2017.05.039
28. Mo, X.; Huang, J.; Sun, Y.; Chen, X.; Deng, Y.; Liu, C.; Jin, W.; Nie, J.; Zhang, Y. Simple, rapid, portable and quantitative sensing of Fe^{3+} ions via analyte-triggered redox reactions mediating Tyndall effect enhancement of Au nanoparticles. Microchemical Journal, 2022, 174, 107075. https://doi.org/10.1016/j.microc.2021.107075
29. Jin, C.; Yang, S.; Zheng, J.; Chai, F.; Tian, M. Paper-based triple-readout nanosensor for point-of-care detection of glucose in urine. Biosensors and Bioelectronics, 2025, 269, 116931. https://doi.org/10.1016/j.bios.2024.116931
30. Xu, S.; Zhang, H.; Qian, Z.; Yuan, W. pH-Responsive injectable self-healing hydrogels loading Au nanoparticles-decorated bimetallic organic frameworks for synergistic sonodynamic-chemodynamic-starvation-chemo therapy of cancer. Journal of Colloid and Interface Science, 2024, 675, 746–760. https://doi.org/10.1016/j.jcis.2024.07.039
31. Dai, Y.; Wen, X.; Fan, H.; Hong, J.; Huang, L.; Zhang, Q.; Xu, J.; Zhang, J.; Zhang, H.; Zhu, W.; Hong, J. Carbon Dots Dually Doped with Fe and Co for Visual Detection of H_2O_2 and Glutathione. ACS Appl. Nano Mater., 2024, 7, 17795–17803. https://doi.org/10.1021/acsanm.4c03016
32. Li, Y.; Qu, C.; Ye, Q.; Meng, F.; Yang, D.; Wang, L. Enhanced tetracycline degradation by novel Mn–FeOOH/CNNS photocatalysts in a visible-light-driven photocatalysis coupled peroxydisulfate system. Environ. Res., 2024, 257, 119293. https://doi.org/10.1016/j.envres.2024.119293
33. Wang, C.; Wang, Z.; Zeng, B.; Zheng, M.; Xiao, N.; Zhao, Z. Fenton-like reaction of the iron(II)–histidine complex generates hydroxyl radicals: implications for oxidative stress and Alzheimer's disease. Chem. Commun., 2021, 57, 12293–12296. https://doi.org/10.1039/D1CC05000A

Supplementary Files

This is a list of supplementary files associated with this preprint. Click to download.

- Supplementarymaterial.docx
- Graphicalabstract.png